PHILOSOPHICAL TRANSACTIONS A

rsta.royalsocietypublishing.org

Research

Article submitted to journal

Subject Areas:
xxxxx, xxxxx, xxxx

Keywords:
mushy layer, sea ice, solidification, convection

Author for correspondence:
Andrew J. Wells
e-mail:
andrew.wells@physics.ox.ac.uk

Mushy layer growth and convection, with application to sea ice

Andrew J. Wells[1], Joseph R. Hitchen[1] and James R. G. Parkinson[1]

[1] Department of Physics, University of Oxford, Clarendon Lab, Parks Road, Oxford, OX1 3PU, UK.

Sea ice is a reactive porous medium of ice crystals and liquid brine, which is an example of a mushy layer. The phase behaviour of sea ice controls the evolving material properties and fluid transport through the porous ice, with consequences for ice growth, brine drainage from the ice to provide buoyancy fluxes for the polar oceans, and sea-ice biogeochemistry. We review work on the growth of mushy layers and convective flows driven by density gradients in the interstitial fluid. After introducing the fundamentals of mushy-layer theory, we discuss the effective thermal properties including the impact of salt transport on mushy-layer growth. We present a simplified model for diffusively controlled growth of mushy layers with modest cooling versus the solutal freezing-point depression. For growth from a cold isothermal boundary, salt diffusion modifies mushy layer growth by around 5-20% depending on the far-field temperature and salinity. We also review work on the onset, spatial localisation and nonlinear development of convective flows in mushy layers, highlighting recent work on transient solidification and models of nonlinear convection with dissolved solid-free brine channels. Finally, future research opportunities are identified, motivated by geophysical observations of ice growth.

1. Introduction

Each winter, large regions of the polar oceans freeze over to form sea ice, with implications for climate and biology in the polar regions and beyond [1]. The freezing of saline ocean water results in a reactive porous mushy layer of ice crystals and interstitial brine [2]. The porosity of sea ice modifies the material properties, provides a substrate for biogeochemical activity, and can

THE ROYAL SOCIETY PUBLISHING

provide pathways for transport between the ice, ocean and atmosphere (see reviews by [1,3,4]). In particular, convection of dense interstitial brine from the ice controls buoyancy fluxes which drive ocean mixing and circulation [3,5]. Hence, understanding the growth and fluid flow through porous mushy layers is of considerable interest.

The goal of this article is to review recent developments in understanding of the growth of mushy layers and multiphase convective transport within them. We also describe new results on the impact of solute diffusion on mushy layer growth. The dynamics of reactive porous materials have broad implications in geophysical and engineering settings [6], and we will take a general fluid-dynamical approach to the underlying theory and experiments, but will exemplify sea ice as a case study. Several previous reviews have treated the fundamentals of convection in mushy layers [6,7] and its application to sea ice growth and parameterisations of brine drainage [3,5]. After introducing the key concepts, we update on recent work and highlight key uncertainties, with particular emphasis on the impact of salt diffusion on the effective properties of mushy layers, and the confinement of convection during transient growth. Due to restrictions on article length, our literature review illustrates key insights rather than being exhaustive.

Section 2 introduces the theory of mushy layer growth, with a discussion of effective material properties and new calculations in §2(c) illustrating the impact of salt diffusion on diffusively controlled mushy-layer growth. Section 3 considers convection in mushy layers, reviewing basic phenomenology, convective onset, the nonlinear development of convection and formation of brine channels, and open questions raised by field observations of brine rejection and biogeochemical transport. We conclude with future perspectives in §4.

2. Theory of mushy layer growth

(a) Fundamentals

Mushy layers are multiphase porous mixtures of solid crystals and interstitial solution with salinity or solute concentration S and temperature T, formed by the solidification of a multicomponent solution. We illustrate the key concepts here for a binary solution with eutectic temperature T_E at concentration S_E (Fig. 1). We will focus on sub-eutectic solutions (with $S < S_E$) in the theory below for clarity, although the key ideas straightforwardly extend to super-eutectic solutions (with $S > S_E$ and a reversed direction of compositional buoyancy). The leading-order phase behaviour of warm sea ice is often approximated as a sub-eutectic binary solution of fresh ice crystals and saline brine (predominantly NaCl salt), although crystallisation of other chemical compounds may become significant at colder temperatures [3]. When cooled from above, higher salinity brine in the pore matrix has greater density and may be negatively buoyant with respect to the surrounding fluid. A common approach for modelling the thermodynamics of mushy layers is described in [7] with key features summarised below.

Models usually assume that the interstitial fluid is in a local thermodynamic equilibrium, with temperature constrained to the salinity-dependent freezing point given by a liquidus relation $T = T_L(S)$. Due to the large specific surface area of the porous microstructure and narrow pores, any gradients in temperature and salinity on the pore scale can rapidly be equilibrated by pore-scale transport and internal phase change, faster than the timescales of macroscopic transport. This phase equilibrium links T and S, with the volumetric solid fraction ϕ evolving in response to macroscopic transport of heat and salt. Such behaviour gives rise to interesting effective transport properties, as discussed in §2(b)-(c). Accounting for advection, diffusion and latent heat released by internal phase changes, conservation of energy for the multiphase mixture yields

$$\overline{\rho c_p}\frac{\partial T}{\partial t} + \rho_l c_l \mathbf{u}\cdot\nabla T = \nabla\cdot\left(\overline{k}\nabla T\right) + \rho_s L\frac{\partial \phi}{\partial t}, \tag{2.1}$$

where ρ_s and ρ_l are solid and liquid densities, c_l is the liquid specific heat capacity, and L the latent heat of fusion per unit volume. The phase weighted heat capacity $\overline{\rho c_p}$ and phase-weighted

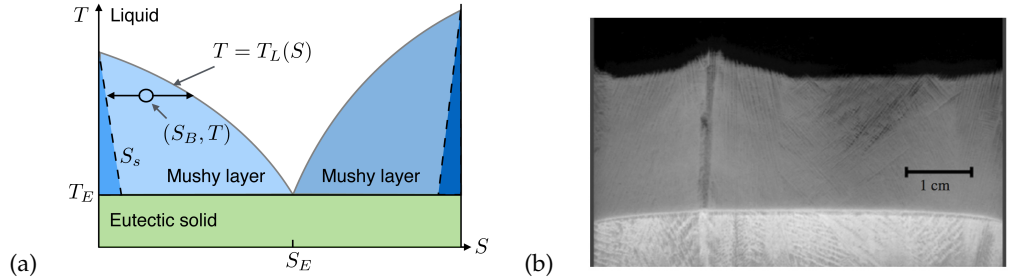

Figure 1. (a) Cartoon phase diagram for a binary solution of concentration S and temperature T. The circular parcel of bulk composition $S_B = S(1-\phi) + S_s\phi$ is a mixture of solid crystals with volumetric solid fraction ϕ and salinity S_s at the solidus (dashed line), and interstitial fluid in phase equilibrium with liquidus temperature $T = T_L(S)$ (grey curves). A sub-eutectic solution (with $S < S_E$) that is cooled first forms a mushy layer of solid solvent crystals and saline interstitial fluid, whilst the salt crystalises into a solid matrix for a super-eutectic solution (with $S > S_E$) leaving a solute-depleted interstitial fluid. A eutectic solid forms below the eutectic temperature T_E. (b) Solidification of a super-eutectic NH_4Cl-H_2O solution cooled from below in a 0.32 mm thick Hele-Shaw cell gives rise to a porous mushy region separating a eutectic solid (light coloured region at bottom) and overlying fluid (dark region). Variations in porosity are evident with darker regions indicating higher porosity, include a steep-sided channel formed by dissolution and convective flow of the buoyant solute-depleted interstitial fluid. Note that the purely liquid channel here only partially fills the cell width, with some crystallisation against the back wall. Image from [8]

thermal conductivity $\overline{k}$ both depend on ϕ. The second term in (2.1) describes advective transport by the Darcy velocity $\mathbf{u} = (1-\phi)\mathbf{v}$, where $\mathbf{v}$ is the interstitial velocity. The corresponding phase-weighted equation for conservation of solute is

$$\frac{\partial}{\partial t}\left[\rho_l(1-\phi)S + \rho_s\phi S_s\right] + \nabla\cdot(\rho_l\mathbf{u}S) = \nabla\cdot\left(\rho_l\overline{D}\nabla S\right), \tag{2.2}$$

where the solid has concentration $S_s \approx 0$ for sea ice, and the phase weighted diffusivity $\overline{D} \approx D(1-\phi)$ for salt diffusivity D in the liquid. Salt diffusion in the solid is much slower than in the liquid, and is usually neglected. Salinity and temperature are coupled via $T = T_L(S)$ within a mushy layer, and hence (2.1) and (2.2) are effectively two partial differential equations to constrain T and ϕ. Conservation of mass for the two-phase medium of fluid and solid yields

$$\frac{\partial}{\partial t}\left[\rho_l(1-\phi) + \rho_s\phi\right] + \nabla\cdot(\rho_l\mathbf{u}) = 0. \tag{2.3}$$

If $\rho_s \approx \rho_l \approx$ constant then $\nabla\cdot\mathbf{u} \approx 0$ and the Darcy flux is incompressible. Otherwise, differences in density between solid and liquid can drive expansion or contraction flows [9].

One of the challenges in modelling transport through mushy layers is determining an accurate description of flow through the porous matrix. Flow through sea ice can be driven by pressure gradients (such as the hydrostatic head of surface melt ponds that drives flushing; reviewed by [10]) or by buoyancy from density gradients (such as dense interstitial brine convecting into the ocean, as discussed in §3). Flow in a porous material is often described using Darcy's law

$$\mu\mathbf{u}/\Pi = -\nabla p - \rho\mathbf{g}, \tag{2.4}$$

where μ is the dynamic viscosity of the fluid, p the pressure, and $\mathbf{g}$ the gravitational acceleration. The Boussinesq approximation is often invoked, with the fluid density ρ taken as a function of concentration and temperature in the buoyancy force in (2.4), but approximated as a constant ρ_l in all other material properties. The permeability Π depends on the porous microstructure, and is usually taken as a function of ϕ (or porosity $\chi = 1-\phi$). Hence the permeability evolves in response to changing T and S. The functional dependence $\Pi(\chi)$ is hard to effectively constrain, because common measurement techniques drive flow through the porous material, with the resulting transport and reaction modifying χ. With this caveat, Freitag used bail tests with sea

ice [11] to determine an approximate dependence $\Pi = \Pi_1 \chi^{3.1}$ for constant Π_1. This resembles the leading-order behaviour for $\chi \ll 1$ of the classical Carmen-Kozeney relation $\Pi = \Pi_1 \chi^3/(1-\chi)^2$. Alternatively, arguments based on stability criteria for the onset of convection suggest that whilst the Freitag relationship holds for the depth-integrated permeability, a relationship $\Pi = \Pi_1 \chi^2$ may be more appropriate for the local permeability [12]. A potential percolation transition has been suggested, with sea ice becoming relatively impermeable at very small porosity with $\chi < 5\%$ due to a reduction in the connectivity of pores [13]. The behaviour as $\chi \to 1$ remains relatively untested, and may be important for flow through highly permeable sea ice near to the mush-liquid interface. In models it is often desirable to describe a continuous transition between Darcy flow in a porous medium and the Navier-Stokes equation in pure liquid, in which case a Darcy-Brinkman momentum equation has been applied [14].

(b) Effective properties of a mushy layer

The local internal phase equilibrium leads to effective thermal properties of a mushy layer, as a result of combined heat and solute transport. An equation for $\partial\phi/\partial t$ can be obtained by approximating ρ_s, ρ_l and S_s as constants, using (2.3) to eliminate $\nabla \cdot \mathbf{u}$ in (2.2) and expanding the time derivative. Substituting this into (2.1) yields

$$(\rho c_p)_{\mathrm{m,eff}} \frac{\partial T}{\partial t} + (\rho c_p)_{\mathrm{l,eff}} \mathbf{u} \cdot \nabla T = \nabla \cdot \left(\overline{k} \nabla T\right) + \frac{\rho_l L}{(S_s - S)} \nabla \cdot \left[D\chi \frac{dS}{dT} \nabla T \right]. \tag{2.5}$$

Here dS/dT is determined from the liquidus function $T = T_L(S)$ and the effective heat capacities

$$(\rho c_p)_{\mathrm{m,eff}} = \overline{\rho c_p} + \frac{\rho_l L \chi}{(S_s - S)} \frac{dS}{dT}, \qquad (\rho c_p)_{\mathrm{l,eff}} = \rho_l c_l + \frac{\rho_l L}{(S_s - S)} \frac{dS}{dT}, \tag{2.6}$$

implicitly account for the release or absorption of latent heat as χ evolves via internal phase change [2,15]. When written in terms of T and the bulk salinity $S_B \approx S\chi$ with $S_s \approx 0$, the effective mushy-layer heat capacity $(\rho c_p)_{\mathrm{m,eff}}$ recovers the form commonly used in models for sea ice growth (see [2]). The last term in (2.5) reflects the coupling of diffusive salt fluxes and heat fluxes arising from internal phase equilibrium. Using the liquidus relation, one can show that a diffusive salt flux $-D\chi\nabla S = -D\chi(dS/dT)\nabla T$ occurs whenever there is a thermal gradient. This linkage has previously been recognised as a mechanism for brine pocket diffusion in sea ice (reviewed in [10]). However, recent work [15,16] noted the converse property: salt diffusion drives a modest but non-negligible thermal transport. In §2(c) we describe a simplified approximate model for low solid fraction, that characterises this transport via an effective enhanced thermal conductivity.

The linkage between thermal gradients and diffusive salt transport also implies some peculiarities near boundaries subject to a cooling heat flux, which require a corresponding diffusive salt flux across the boundary if the material is to remain mushy and in local thermodynamic equilibrium. If there is no source of salt at the boundary to supply this flux, the mush desalinates and forms a thin layer of pure solid at the boundary [17,18]. If such conditions were realised at the upper surface of sea ice, this would generate an entirely solid crust that is impermeable to significant biogeochemical fluxes and gas exchange between the sea ice pore space and the atmosphere. However, the salinity conditions at the sea-ice surface potentially features a 3 phase problem between ice, liquid brine and air which remains poorly understood, with observations of surface brine layers during early growth [19].

(c) Impact of salt diffusion on mushy layer growth

In this section we describe a simplified model for diffusive growth of a sub-eutectic mushy layer (with $\mathbf{u} = 0$). A deep layer of fluid with initial temperature T_∞ and salinity S_∞ is cooled from below with boundary temperature T_0 at $z = 0$. We assume a linear liquidus $T_L(S) = T_0 - \Gamma(S - S_0)$ for constant Γ, where the boundary composition S_0 satisfies $T_0 = T_L(S_0)$. For simplicity in what follows we assume that the solid concentration S_s is constant, and independent of temperature. The asymptotic simplification considers a limit where the concentration ratio

$\mathcal{C} \equiv [S_\infty - S_s] / [S_0 - S_\infty] = [T_L(S_s) - T_L(S_\infty)] / [T_L(S_\infty) - T_0] \gg 1$. Note that we here define $\mathcal{C}$ in terms of a general boundary temperature. This generalises previous work which used $T_0 \approx T_E = T_L(S_E)$, such that $\mathcal{C} \gg 1$ describes a near-eutectic limit [6]. For sea ice, with typical values $T_L(S_\infty) \approx -2^\circ\mathrm{C}$ and $T_L(S_s) \approx 0^\circ\mathrm{C}$, it requires boundary temperatures T_0 sufficiently close to the freezing temperature $T_L(S_\infty)$ of the far field fluid. Whilst not typical for sea ice growth in the field, the limit $\mathcal{C} \gg 1$ is pursued here to provide conceptual insight. We also assume that solute diffusion is weak but not completely negligible compared to thermal diffusion (specifically, we assume that the Lewis number $Le = \kappa/D \gg 1$ for thermal diffusivity κ, but with terms of order $(D/\kappa)L/c_p\Gamma(S_\infty - S_s)$ retained). A detailed analysis is described in [16], but we here highlight the main results via a heuristic approach.

The above assumptions lead to a small solid fraction in the mushy layer $\phi \ll 1$, which is rationalised as follows. We define the bulk phase-weighted salinity of a fluid parcel as $S_B = S(1-\phi) + S_s\phi$. If solute diffusion is weak in (2.2) then to leading order the bulk salinity $S_B \approx S_\infty$ remains close to the initial value, with a weak higher order correction due to solutal diffusion. Then rearranging yields $\phi \approx [S - S_\infty] / [S - S_s] = [T_L(S_\infty) - T] / [T_L(S_s) - T]$. Noting that the mush temperature lies between the values at the boundary and the freezing point of the far-field liquid $T_0 < T < T_L(S_\infty)$, then the condition $\mathcal{C} \gg 1$ implies $\phi \ll 1$. Thus we can approximate $\chi \approx 1$ in the effective material properties (2.6), and to leading order the expression for bulk salinity yields $S \approx S_B \approx S_\infty$ in (2.5) and (2.6). This neglects higher order corrections of $\mathcal{O}(\phi)$. N.B. we have here neglected D/κ when approximating ϕ, but retain it in the thermal equation (2.5) where it is multiplied by a large contribution from latent heating - this approximation can be verified a posteriori [16]. Invoking these approximations (2.5) yields

$$\frac{\partial T}{\partial t} = \kappa_m \frac{\partial^2 T}{\partial z^2}, \qquad \kappa_m \equiv \kappa \frac{[1 + (D/\kappa)L/c_p\Gamma(S_\infty - S_s)]}{[1 + L/c_p\Gamma(S_\infty - S_s)]}. \tag{2.7}$$

The effective mushy-layer diffusivity κ_m highlights the impact of phase equilibrium on thermal transport in mushy layers. The denominator shows that thermal diffusion is weakened by a factor $\Omega = 1 + L/c_p\Gamma(S_\infty - S_s)$ due to an enhanced effective heat capacity from the latent heating from internal phase changes [20]. Thermal diffusion is also enhanced by a factor $1 + (D/\kappa)L/c_p\Gamma(S_\infty - S_s)$ due to salt diffusion which drives local solidification/dissolution of the solid matrix and latent heat release/uptake in order to maintain phase equilibrium [15,16]. Whilst the impact of weak salt diffusion has commonly been neglected on account of $D/\kappa \ll 1$, this analysis suggests that salt diffusion can still have a significant impact if $(D/\kappa)L/c_p\Gamma(S_\infty - S_s)$ is not too small. For sea ice formation from saltwater of $S_\infty \approx 35\mathrm{g\,kg}^{-1}$, $D/\kappa \approx 1/200$, whilst $L/c_p\Gamma(S_\infty - S_s) \approx 40$, implying that salt diffusion will boost the effective mushy layer diffusivity by a factor of order 20% compared to evaluating κ_m with $D = 0$.

The resulting impact of salt diffusion on mushy layer growth is illustrated by solving the Stefan problem governed by (2.7) and $T = T_L(S)$ in a mushy region $0 < z < h(t)$, where $h(t)$ is the mushy layer thickness. Temperature and salinity decouple in the liquid region, with

$$\frac{\partial T}{\partial t} = \kappa \frac{\partial^2 T}{\partial z^2}, \qquad \frac{\partial S}{\partial t} = D \frac{\partial^2 S}{\partial z^2}, \qquad z > h(t). \tag{2.8}$$

We assume far-field boundary conditions $S \to S_\infty$ and $T \to T_\infty$ as $z \to \infty$. The boundary conditions at the mush-liquid interface need more careful justification. Because the underlying solute equation (2.2) behaves as a hyperbolic equation for ϕ in the mushy region, the boundary conditions depend on whether characteristic paths for ϕ advance from the moving interface into the mush, or conversely from the mush to intersect the interface (see [18,21] for a detailed discussion). Here the interface advances rapidly controlled by thermal diffusion, compared to characteristic speeds for ϕ which are controlled by solute diffusion, and a closure condition is required to determine the interface position $z = h(t)$. We apply a condition of marginal equilibrium with $\mathbf{n} \cdot \nabla T = \mathbf{n} \cdot \nabla T_L(S)$ in the liquid at the mush-liquid interface $z = h$ with unit normal $\mathbf{n}$, so that the mush advances to just remove supercooling in the liquid [17]. Continuity of temperature, salinity, heat flux and solute flux at the interface yields $[T]^+_- = [S]^+_- = [\mathbf{n} \cdot \nabla T]^+_- =$

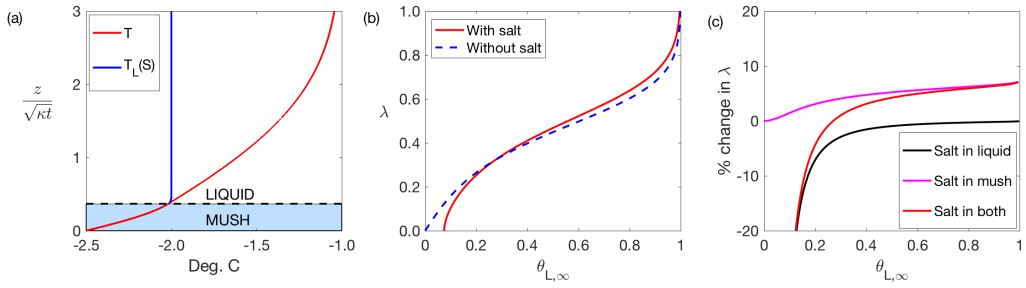

Figure 2. (a) Solution of the simplified model for mushy layer growth with thickness $h(t) = \lambda\sqrt{\kappa t}$ when a liquid of far field temperature T_∞ and salinity S_∞ is cooled from below by a boundary of temperature T_0 at $z = 0$. The temperature T and liquidus temperature of the liquid salinity $T_L(S)$ are plotted as functions of depth normalised by the diffusion length $z/\sqrt{\kappa t}$ for solidification of seawater with $T_0 = -2.5^\circ$C, $T_\infty = -1^\circ$C, $T_L(S_\infty) = -2^\circ$C. (b) Variation of the scaled mushy-layer thickness $\lambda = h(t)/\sqrt{\kappa t}$ with thermal conditions characterised by $\theta_{L_\infty} = [T_L\,(S_\infty) - T_0]\,/\,[T_\infty - T_0]$. The solution with salt diffusion included in the model (solid curve), shows modest differences to a solution that neglects salt diffusion with $Le \to \infty$ (dashed curve). (c) Difference between solutions including various components of salt diffusion relative to the solution with salt diffusion entirely neglected. The full solution including salt diffusion (red curve) transitions between limiting cases where the effect of salt diffusion is retained in the liquid $z > h$ but neglected in the mush $z < h$ (black curve), and where salt diffusion is retained in the mush but neglected in the liquid (magenta curve).

$[\mathbf{n}\cdot\nabla S]^+_- = 0$ at $z = h(t)$ where we use square brackets in this equation to denote jump conditions at the interface. The cooled lower boundary is isothermal with $T = T_0$ at $z = 0$. For simplicity we here assume that the lower boundary is maintained at the constant salinity S_0. If a condition of no salt flux were instead applied at $z = 0$, the diffusion of salt away from this boundary would lead to a thin layer of pure solid [17], with the approximation $\phi \ll 1$ breaking down in the vicinity of this region.

With the above boundary conditions, a self similar solution to (2.7) and (2.8) can be found:

$$T = \begin{cases} T_0 + (T_\infty - T_0)\,\alpha\,\mathrm{erf}\left(\frac{z}{2\sqrt{\kappa_m t}}\right), & z \le h, \\ T_\infty + (T_\infty - T_0)\left[\alpha\,\mathrm{erf}\left(\frac{\lambda}{2}\sqrt{\frac{\kappa}{\kappa_m}}\right) - 1\right]\frac{\mathrm{erfc}\left(\frac{z}{2\sqrt{\kappa t}}\right)}{\mathrm{erfc}\left(\frac{\lambda}{2}\right)}, & z > h, \end{cases} \tag{2.9}$$

$$S = S_\infty + \frac{\left[T_L\,(S_\infty) - T_0 - (T_\infty - T_0)\,\alpha\,\mathrm{erf}\left(\frac{\lambda}{2}\sqrt{\frac{\kappa}{\kappa_m}}\right)\right]}{\Gamma}\frac{\mathrm{erfc}\left(\frac{z}{2\sqrt{Dt}}\right)}{\mathrm{erfc}\left(\frac{\lambda}{2}\sqrt{\frac{\kappa}{D}}\right)}, \quad z > h, \tag{2.10}$$

(see Fig. 2) and the mush thickness $h(t) = \lambda\sqrt{\kappa t}$ grows over time proportional to the thermal diffusion length. The constant α satisfies

$$\alpha^{-1} = \mathrm{erfcx}\,(\lambda/2)\,\sqrt{\kappa/\kappa_m}\,\exp\left[-(\lambda^2/4)(\kappa/\kappa_m)\right] + \mathrm{erf}\left[\lambda\sqrt{\kappa/\kappa_m}/2\right], \tag{2.11}$$

where

$$\mathrm{erf}(\zeta) = \frac{2}{\sqrt{\pi}}\int_0^\zeta \exp(-u^2)\,du, \qquad \mathrm{erfc}(\zeta) = 1 - \mathrm{erf}(\zeta), \qquad \mathrm{erfcx}(\zeta) = \mathrm{erfc}(\zeta)\,\exp\left(\zeta^2\right). \tag{2.12}$$

The scaled growth rate λ satisfies

$$\theta_{L_\infty}\mathrm{erfcx}\left(\frac{\lambda}{2}\right) + (\theta_{L_\infty} - 1)\sqrt{\frac{\kappa_m}{\kappa}}\mathrm{erf}\left(\frac{\lambda}{2}\sqrt{\frac{\kappa}{\kappa_m}}\right)\exp\left(\frac{\kappa}{\kappa_m}\frac{\lambda^2}{4}\right) = \sqrt{\frac{D}{\kappa}}\mathrm{erfcx}\left(\frac{\lambda}{2}\sqrt{\frac{\kappa}{D}}\right) \tag{2.13}$$

and in figure 2(b) is plotted as function of $\theta_{L_\infty} = [T_L\,(S_\infty) - T_0]\,/\,[T_\infty - T_0]$ which characterises the relative significance of the freezing temperature of the far-field fluid versus the far-field temperature, both measured relative to the cooling temperature T_0. Solute diffusion has two impacts on mushy layer growth. The impact on the effective thermal diffusivity is carried by

the dependence of κ_m on $Le = \kappa/D$ on the left hand side of (2.13). A diffusive solutal boundary layer can also develop at the mush-liquid interface, leading to the Le-dependent term on the right hand side of (2.13). The red line in figure 2(c) shows the fractional change due to inclusion of solute diffusion (i.e. finite Le) which transitions between two limits. For small θ_{L_∞} the liquid is significantly warmer than its salinity-dependent freezing point and the impact of the solutal boundary layer dominates, as indicated by approach to a solution (black line) that neglects the effect of salt diffusion in κ_m but retains it in the liquid. Slow diffusion allows solute to build up ahead of the solidification front and depresses the freezing temperature, slowing growth. For larger θ_{L_∞} the liquid is closer to its freezing point and solute diffusion in the mushy layer dominates and enhances growth, as indicated by approach to the magenta line calculated by neglecting salt diffusion in the liquid, but retaining it in the mush. Overall, these solutions illustrate that solute diffusion has a modest impact on the mushy-layer growth rate.

3. Convection in mushy layers

Detailed reviews of convection in mushy layers are given in [3,5,6]. In this section we will briefly summarise key concepts and observational phenomenology, before updating on recent developments on modelling of convection during steady and transient ice growth, and comparison to experimental and computational approaches. We conclude with potential future research questions motivated by geophysical observations and biogeochemical transport.

(a) Phenomenology of convection in mushy layers

Convection in mushy layers is driven by density gradients in the interstitial liquid arising from thermal gradients and coupling to S via local phase equilibrium [6]. For sea ice, the resulting convective flow acts to drive salt fluxes to the ocean, a process often called gravity drainage [3,5]. Experiments show that convection within the interior of a mushy layer usually leads to the formation of solid-free chimneys (called brine channels in the case of sea ice), both in steady state growth [8,22,23] and transient growth settings (e.g. [24–26] and results reviewed by [6]). Such brine channels result from a reactive flow-focusing instability [6]. In the case of sea ice growth, sinking highly saline brine is out of equilibrium with the background solid and temperature conditions, and dissolves solid ice crystals, increasing the porosity and permeability, and leading to focusing of flow into the narrow high permeability channel. Dye tracing reveals a slower broader return flow between the narrow brine channels [27]. Brine channels have been directly observed via post mortem measurements or observations of convective plumes draining from the ice (e.g. [28] and other work reviewed by [3,6]), whilst channels in an actively solidifying mushy layer have been imaged during growth using Magnetic Resonance Image scanning [29]. During transient growth, the pattern of convection and brine channels evolves as the mushy layer thickens. A coarsening of the mean brine channel spacing has been observed [24,26,30]. There is also evidence of localisation of solute transport in an actively convecting region near the mush-liquid interface, while deeper parts of the mushy layer have higher solid fraction and lower permeability after solute rejection [10,29]. Post mortem measurements of sea ice cores also suggest this results in a basal layer with higher salinity gradient, whilst the upper ice approaches a stable bulk salinity that increases weakly with the growth rate (e.g. discussed in [31]).

(b) Onset of convection in mushy layers

Understanding the conditions for the onset of convection provides fundamental dynamical insight, and helps to constrain parameterisation schemes of salt transport [5]. A wide body of work reviewed in [6] uses linear and weakly-nonlinear stability analyses to study the onset of convection during steady-state growth, such as directional solidification where a sample is pulled at constant speed between heat exchangers. Two modes of instability are observed: mushy-layer mode convection is driven by density gradients within the mush, whilst boundary-layer

convection features instability of the compositional boundary layer in the liquid ahead of the growing mush. The latter has smaller wavelength, and shallower penetration into the mush. Both modes have been observed in experiments, with increasing solution viscosity promoting the significance of the boundary layer mode [30]. The onset of mushy-layer mode convection can be characterised in terms of a mushy-layer Rayleigh number $R_m = g\Delta\rho\Pi_1 h/\mu\kappa$ exceeding a critical value dependent on other parameters such as the Stefan number $\mathcal{S} = L/c_p\Delta T$ and the concentration ratio $\mathcal{C}$. Here g is the gravitational acceleration, ΔT and $\Delta\rho$ are the temperature and density differences across the mushy layer, Π_1 the reference permeability, and h a characteristic lengthscale (with $h \sim \kappa/V$ for directional solidification at imposed growth rate V). The mushy-layer Rayleigh number characterises the ratio of buoyancy forcing to dissipative mechanisms, and can be interpreted as a ratio of two timescales. Invoking a balance between buoyancy forces and viscous drag in the porous media yields a velocity scale $g\Delta\rho\Pi_1/\mu$, and timescale $\tau_a \sim \mu h/g\Delta\rho\Pi_1$ for flow across the mushy layer. Full depth buoyancy anomalies are predominantly dissipated by thermal diffusion over a timescale $\tau_d \sim h^2/\kappa$, with temperature changes causing salinity changes to maintain phase equilibrium. If $\tau_a \ll \tau_d$ then buoyancy anomalies are advected through the mushy layer before they are dissipated, and convection occurs. Alternative interpretations exist that capture the same underlying ratio of buoyancy and dissipation, such as using energetics of parcel displacements [5]. Note that the classical form of double diffusive instability is ruled out in mushy layers due to the coupling of T and S imposed by local thermodynamic equilibrium [20].

Stability analyses for small amplitude disturbances to a background state of steady diffusive growth suggest that the convective instabilities can either be a direct exchange of instability (featuring pure exponential growth), or for certain ranges of $\mathcal{C}$ and $\mathcal{S}$ can be oscillatory with lagged feedbacks between developing flow and porosity [6]. The resulting deformation of the mush-liquid interface also has a destabilising influence [32]. Shear flow in the underlying fluid can enhance convective instability [33,34], or drive flow-focusing instabilities entirely independent of convection [35,36]. Weakly nonlinear analyses provide insight into pattern formation [6] and the potential for interactions between modes leading to travelling or standing waves [37,38]. For certain growth parameters, the bifurcations are subcritical [6] leading to the possibility of onset of convection at smaller Rayleigh numbers via finite amplitude disturbances (e.g. see numerically computed states with brine channels by [39–41]). Approaches to estimating nonlinear optimal perturbations [42] and rigorous lower bounds on stability [43] have proven fruitful in other hydrodynamical stability problems, and this might be an interesting opportunity for future exploration. Experimental observations of NH_4Cl-H_2O mushy layers show that convection occurs for sufficiently high liquid concentration, or sufficiently low growth rate, qualitatively consistent with a critical Rayleigh number [22]. There have also been observations of oscillatory dynamics, with plumes from channels oscillating either in phase [22] or out of phase [24].

Instabilities also occur in ternary alloys with three chemical constituents (see work reviewed in [44]). In addition to convective instabilities similar to those discussed above, ternary alloys feature new modes due to the coupling of phase changes of different components using the extra degree of freedom provided by a three-dimensional phase diagram for T and two compositions, and formation of a primary solid phase alone.

Whilst steady-state growth provides valuable conceptual insight, sea-ice growth is often transient with both the mushy-layer thickness and cooling conditions evolving over time. Studying convective stability during transient growth presents new mathematical challenges, since both the background state and perturbations evolve over time. This issue has been extensively studied for convection in a porous medium with a growing diffusive boundary layer. A variety of methods yield broadly similar results for the underlying physical lengthscales, but with some differences in the numerical prefactors (see discussion in [45]). The linear convective instability during mushy layer growth has been examined in so-called fixed chill settings with a deep fluid layer cooled by an isothermal boundary. Analysis in a near-eutectic limit $\mathcal{C} \gg 1$ with low solid fraction yields a critical mushy-layer Rayleigh number of order 10-20, where the mush thickness $h \propto \sqrt{\kappa t}$ depends on the thermal diffusion lengthscale controlling

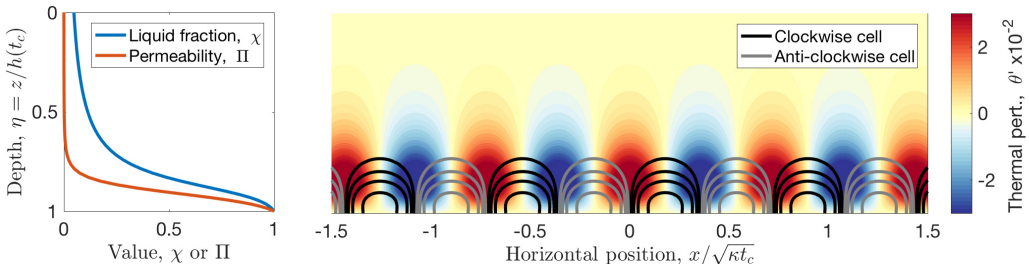

Figure 3. Left: variation of background liquid fraction χ and dimensionless permeability $\Pi = \chi^3$ with depth normalised by mushy layer thickness h. The solution is evaluated at the critical time t_c for onset of convection, for diffusive growth of sea ice from a cooled upper boundary of temperature $T_0 = -16°\mathrm{C}$ into a fluid with far-field temperature $T_\infty = 0°\mathrm{C}$ and liquidus temperature $T_L(S_\infty) = -0.84°\mathrm{C}$, with $L/c_l = 80°\mathrm{C}$. This yields $\mathcal{C} = 0.05$, $\theta_{L,\infty} = 0.95$. Right: equally spaced contours of the perturbation streamfunction (grey/black curves) and dimensionless temperature perturbation $\theta' = T'/\Delta T$ (colour scale, for arbitrary temperature scale ΔT) at the critical Rayleigh number and wavenumber for the onset of convection, observed at time t_c. The liquid fraction χ and temperature T in the background state are determined by solving (2.1) and (2.2) for an ideal mushy layer with uniform material properties and $D = \mathbf{u} = 0$, whilst the perturbations are calculated from a linear stability analysis for growth of convective perturbations described by Darcy's law (2.4) and a linearisation of (2.1) and (2.2) about the background state of diffusive growth. See [16] for full methodological details.

initial growth (see [46,47] and references therein). Because the solid fraction is low, the linear convective modes easily penetrate through the depth of the mushy layer. The critical Rayleigh number increases significantly as $\mathcal{C}$ decreases [48] and variation of porosity and permeability becomes more significant. For low $\mathcal{C}$ typical of sea ice growth, Hitchen [16] showed that this behaviour can be understood in terms of a localisation of the convection to a high permeability region close to the mush-liquid interface, where the background porosity and permeability vary significantly. Figure 3 illustrates an example of the background porosity and permeability calculated for diffusive sea ice growth from an isothermal cold upper boundary, along with convective perturbations at the critical Rayleigh number and wavenumber from a linear stability analysis (see caption for the methodology). The convective cells penetrate over a depth commensurate with the high permeability region. Whilst only applying to linear perturbations, the analysis of [16] (further details will be reported elsewhere) lends support to previous scaling arguments used to define a depth-dependent critical Rayleigh number $R_m(z) = g\beta\Delta\rho(z)\Pi(z)(h-z)/\kappa\mu$ [10,29] for the parameterised onset of convection in sea ice models [5]. Notably, this predicts localisation of convective flow independent of any percolation transition in the permeability (c.f. [13]). Such flow localisation has important implications for the depth-dependence of the desalination of ice and accompanying biogeochemical fluxes [3].

A delay in the onset of convection is predicted by the stability analyses due to the time taken for the mush to grow sufficiently thick for the Rayleigh number to exceed a critical value. Such a delay is seen in laboratory experiments using fixed chill cooling for solutions with $\mathcal{C} \gg 1$ [30] and $\mathcal{C} \ll 1$ [49]. The boundary temperature varies significantly in field settings for sea ice growth. A delay of convective onset until a few centimetres of ice has grown has been inferred in leads [50]. However, if the ice cools slowly and is initially warmer and more permeable, the predicted delay in convective onset may be too short to be practically observable [10]. A further issue hindering quantitative comparisons is that the permeability remains quantitatively underconstrained. An inverse approach has used observations of ice depth and thermal conditions to infer a permeability that is consistent with the predicted critical Rayleigh number (e.g. see [12,34,49]).

(c) Nonlinear convection with brine channels

The brine fluxes from growing sea ice due to gravity drainage are mediated by nonlinear convective flows through brine channels [3,5]. This presents a challenge for models, which must deal with a transition between flow in a porous mushy region over most of the domain, and through a pure liquid region in the brine channels. One approach uses a split domain formulation, with separate mushy and pure-liquid regions. A hybrid theoretical and numerical approach was developed for steady state growth [39,40]. This uses asymptotic approximations for flow in slender symmetric brine channels, which provides hydrodynamical and thermodynamical boundary conditions for a numerical solution for flow in the mushy region. This approach captures the qualitative structure of asymmetric convection cells observed in experiments, with broad weak upwelling, and strong downflow in narrow channels (e.g. [27]). This hybrid approach has been adapted [41,51] to study the sensitivity of solute fluxes to channel spacing in a 2D periodic geometry. For solidification in wide domains, [41] hypothesised a variational principle where the nonlinear dynamics adjusts to maximise the flux of potential energy from the mushy layer, and predicts a dimensionless solute flux $F_s/(\Delta S\, V) \sim \alpha(Rm - Rm_c)$ that scales linearly with the Rayleigh number for steady state growth at rate V (with Rm_c and α constant). This scaling predicts solute rejection consistent with experiments on the early stages of transient ice growth from an isothermal boundary [52]. A simplified semi-analytical model was developed for the near-eutectic limit [53] which recovers the leading order behaviour seen in the numerical calculations and the strength of convective flow in experiments [54]. Parameterisation schemes for sea ice models have been implemented using these developments (reviewed by [5]). The model of [41] was also used to study the nonlinear dynamics of convection through brine channels. Convection through the brine channels is extinguished either for a low Rayleigh number based on the mushy-layer thickness, or for narrow samples where the sample width provides a relevant controlling lengthscale [51]. The experimentally observed stability threshold for these nonlinear convective states compares well with numerical predictions with a fitted permeability [8].

An alternative approach to modelling mushy-layer convection uses a single-domain enthalpy method (see [3,57] for reviews). The energy and solute equations are solved for enthalpy and bulk solute concentration, with the resulting temperature, liquid salinity and solid fraction inferred from a phase diagram. This approach requires a momentum equation suitable for both porous and liquid regions, with a Darcy-Brinkman equation commonly used [14] or a modified form of Darcy's law exploited for flow in a narrow Hele-Shaw cell [55]. It is challenging to properly resolve the narrow purely liquid brine channels at acceptable computational cost. Many previous simulations result in brine channels contracting to only a few computational grid cells in width [55]. Some of our ongoing work is applying a finite volume code capable of exploiting adaptive mesh refinement [56] to simulate convection with fully resolved brine channels. Figure 4 shows an example simulation of transient mushy-layer growth from an isothermal cooled boundary, where the width of the brine channels is resolved with approximately 10 computational cells. This initial exploratory simulation shows evidence of a coarsening of the spacing of brine channels as the mush layer thickens over time, as observed in experiments of transient solidification (see §3(a)). Fully exploring the nonlinear dynamics of brine channels during transient growth and their resulting solute fluxes remains a topic of ongoing work.

Some features observed in mushy layer experiments remain to be theoretically reconciled. Observed oscillatory modes of convection [22,24] are qualitatively consistent with linear stability analyses, and have been compared to weakly nonlinear analysis in [38]. However the conditions for their occurrence and their impact on solute fluxes have yet to be reconciled in models with finite amplitude flow through brine channels. Channels can also show significant sidebranching [27–29]. It is not clear whether such sidebranching can be explained by continuum models of mushy layers, or might be inherited from the pore scale microstructure.

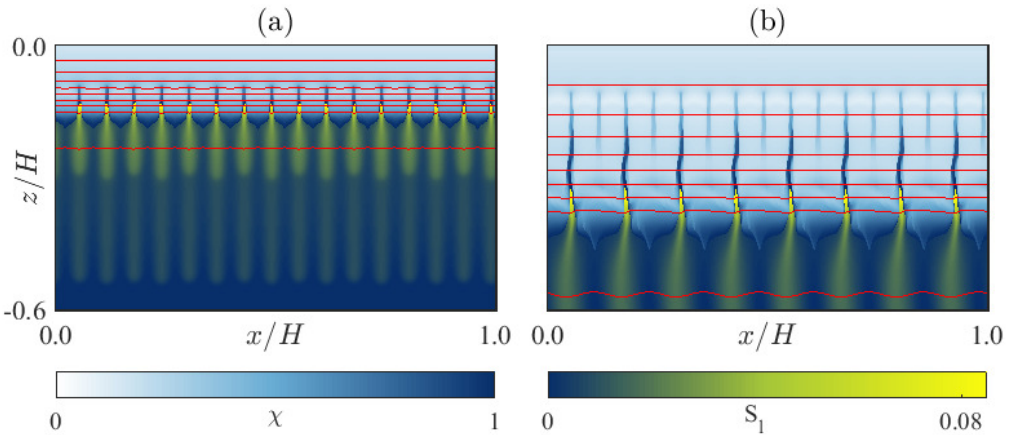

Figure 4. Two snapshots of simulated mushy layer growth for an Na Cl-H_2O solution in a thin, quasi-two dimensional Hele-Shaw cell cooled from above with an isothermal impermeable upper boundary, laterally periodic boundary conditions and an open basal boundary condition at $z = H$. See supplementary movie for the transient evolution. The white-blue colour scale shows porosity χ in the mushy layer, whilst the blue-yellow colour scale shows dimensionless salinity $S_l = (S - S_\infty)/(S_E - S_\infty)$ in the liquid. Red contours are logarithmically spaced isotherms $\theta = \log_{10}(1 + 10j)/\log_{10}(11)$ for $j = 0, 1, \ldots 10$, where the dimensionless temperature $\theta = (T - T_\infty)/(T_E - T_L(S_\infty))$. The simulation parameter values are $\mathcal{C} = 0.18$, $R_m = 320$, $Le = 100$ and $\mathcal{S} = 5$ with surface temperature $T_0 = T_E$, $h = H$ used in the Rayleigh number, and dimensionless permeability $\Pi = \chi^3$ applied throughout the Hele-shaw cell. The numerical computations employ the enthalpy method described in [55] but implemented using a finite volume scheme adapted from [56] applied on a uniform computational grid of 1024^2 cells. Second-order differencing is used in space, with advection treated explicitly via a conservative Godunov method and implicit timestepping of diffusive terms. A pressure-projection method is used to maintain divergence free velocities, and multigrid iteration used for the implicit solves (see [56] for further description of these numerical schemes). (a) At time $t = 0.19H^2/\kappa$ convective saline plumes sink from the mushy region via a nearly periodic array of approximately vertical brine channels dissolved in the mushy layer, with the corresponding heat and solute transport significantly deforming the mush-liquid interface. (b) At the later time $t = 1.33H^2/\kappa$ the mushy layer has grown thicker and the pattern of actively convecting brine channels coarsens with an increase in their mean spacing. Remnant inactive brine channels leave a high porosity residual in the mushy layer.

(d) Outstanding challenges from geophysical observations of convection from sea ice and biogeochemical transport

Observations of growing sea ice and its impact on the polar oceans also raise new questions. Of key interest to oceanographers is the impact of brine rejection on upper ocean mixing. Salt fluxes below sea ice have been estimated from ocean turbulence arrays mounted on thick ice (discussed in [58]), but it remains challenging to capture ocean fluxes during the early stages of ice growth. The net impact on water mass transformation is inferred from oceanographic measurements and reanalyses (e.g. [59,60]). Some recent observations indicate salt fluxes following warming of the ice in spring [61–63]. Scaling arguments and a one-dimensional parameterisation of salt transfer suggest that such desalination could be caused by full-depth convection during ice warming, which increases the porosity and permeability, and thus increases the Rayleigh number [62]. However, this remains to be explored theoretically, and the impact of freshwater release by basal ice melt has yet to be quantified. Turbulence measurements have also captured fine scale brine plumes observed several metres below the ice [61,63] suggesting that some of the brine rejected from ice may travel a significant distance through the ocean mixed layer before completely mixing. It remains an open challenge to theoretically quantify the response of brine rejection to varying atmosphere and ocean forcing, and the ultimate fate of mixing in the upper ocean.

The convective flow and ice porosity also have important implications for biogeochemical transport in the ice [3,4]. Temporal and spatial variations in ice properties modulate convective transport of dissolved species by varying the Rayleigh number, or the permeability to chemical exchange. Chemical fractionation also occurs as the ice cools and increases in solid fraction, leading to concentrations in the brine far above those in the ocean. This promotes biogeochemical activity within the ice, and provides a source of highly-concentrated brine relevant to atmospheric chemistry seeded at the ice surface or via contact with overlying snow [4]. Of particular fluid dynamical interest is the potential for supersaturation and nucleation of gas bubbles within the liquid pore space. This provides an extra buoyancy source [64], but also potentially introduces complications of capillarity and multiphase flow with partial saturation through the pore space. The microstructural properties of sea ice may also influence macroscopic convective flows. The permeability and conductivity of ice is orthotropic due to anisotropy of the underlying crystal growth [1]. Also, whilst we have focused on growth of congelation ice by direct basal freezing, platelet ice can also form by deposition of frazil ice crystals grown in a supercooled ocean. Such platelet ice retains a higher fraction of salt than congelation ice [31] which remains to be explained.

4. Conclusion

Sea ice growth involves formation and evolution of a porous mushy layer of ice and brine, with effective properties due to the coupling of temperature and salinity via local phase equilibrium. The effective heat capacity of sea ice is modified due to latent heat release/uptake during internal phase change, whilst the effective thermal conductivity is boosted by diffusive salt transport and consequent latent heating during equilibration of the ice matrix to a state of local thermodynamic equilibrium. We have presented a simplified model for large concentration ratio $\mathcal{C} \gg 1$. Solute diffusion enhances mushy-layer growth via the above effective conductivity when the neighbouring liquid is close to the freezing point (large θ_{L_∞}), but retards mushy-layer growth via build up of a solutal boundary layer when the salinity-dependent freezing point is far below the far-field temperature (small θ_{L_∞}). Varying temperature, salinity and porosity also drive and moderate convective solute fluxes from mushy layers via an array of brine channels. Stability theory provides an interpretation of the onset of convective flow and its localisation to a high permeability basal layer in sea ice. Nonlinear models of convection predict solute fluxes in steady growth conditions or with isothermal cooling. Open questions remain about the transient dynamics of brine channels, including the occurrence of oscillating modes of convection and response to time varying forcing. In addition, the permeability-porosity relation remains a key uncertainty for direct comparison of experiment and theory without tuning parameters.

Recent observations of sea ice growth suggest new fluid mechanical and thermodynamical challenges to understand. This includes the multiphase flow of gas bubbles through porous ice, chemical fluxes to the atmosphere, the response of brine fluxes to varying ocean forcing, and ultimate mixing of brine plumes injected into the ocean mixed layer. The mushy layer theory discussed here may provide a useful tool to address some of these challenges.

Data Accessibility. Data and code archived at: https://doi.org/10.5281/zenodo.1487990

Authors' Contributions. JRH developed the theoretical model in §2(c) and carried out the stability analysis in figure 3. JRGP developed the simulation code for figure 4. AJW supervised the research, and drafted the manuscript. All authors contributed to editing and enhancing the manuscript.

Competing Interests. The authors declare that they have no competing interests.

Funding. JRH and JRGP acknowledge PhD studentships funded by NERC awards NE/L501530/1, NE/I528493/1 and NE/L002612/1. AJW acknowledges European Union FP7 award PCIG13-GA-2013-618610 SEA-ICE-CFD. AJW and JRGP acknowledge Royal Society International Exchanges Award IE141071.

Acknowledgements. The authors gratefully acknowledge input from Dan Martin and Richard Katz on the development of the simulation code using CHOMBO.

References

1. Thomas DN and Dieckmann, GS. *Sea Ice*. Blackwell, Oxford, 2nd edition, 2010.
2. Feltham DL Untersteiner N, Wettlaufer JS, Worster MG. 2006 Sea ice is a mushy layer. *Geophys. Res. Lett.*, **33**, L14501.
3. Hunke EC, Notz D, Turner AK, Vancoppenolle M. 2011 The multiphase physics of sea ice: a review for model developers. *Cryosphere*, **5**, 989–1009.
4. Vancoppenolle M, Meiners K, Michel C, Bopp L, Brabant F, Carnat G, Delille B, Lannuzel D, Madec G, Moreau S, Tison J-L, van der Merwe P. 2013 Role of sea ice in global biogeochemical cycles: emerging views and challenges. *Quat. Sci. Rev.*, **79**, 207.
5. Worster MG, Rees Jones DW. 2015 Sea-ice thermodynamics and brine drainage. *Phil. Trans. R. Soc. A*, **373**, 20140166.
6. Worster MG. 1997 Convection in mushy layers. *Annu. Rev. Fluid Mech.*, **29**, 91–122, .
7. Worster MG. 2000 *in Perspectives in fluid dynamics: a collective introduction to current research*, pp. 393–446. Cambridge University Press.
8. Zhong J-Q, Fragoso AT, Wells AJ, Wettlaufer JS. 2012 Finite-sample-size effects on convection in mushy layers. *J. Fluid Mech.*, **704**, 89–108.
9. Chiareli AOP, Worster MG. 1995 Flow focusing instability in a solidifying mushy layer. *J. Fluid Mech.*, **297**, 293–305.
10. Notz D, Worster MG. 2009 Desalination processes of sea ice revisited. *J. Geophys. Res.*, **114**, 1–10.
11. Freitag J. 1999 Untersuchungen zur Hydrologie des arktischen Meereises - Konsequenzen fur den kleinskaligen Stofftransport (in German). *Berichte zur Polarforschun*.
12. Rees Jones DW, Worster, MG. 2014 A physically based parameterization of gravity drainage for sea-ice modeling. *J. Geophys. Res. Oceans*, **119**, 5599–5621.
13. Golden KM, Eicken H, Heaton AL, Miner J, Pringle DJ, Zhu J. 2007 Thermal evolution of permeability and microstructure in sea ice. *Geophys. Res. Lett.*, **34**, L16501.
14. Le Bars M, Worster MG. 2006 Interfacial conditions between a pure fluid and a porous medium: implications for binary alloy solidification. *J. Fluid Mech.*, **550**, 149–173.
15. Butler SL. Effective transport rates and transport-induced melting and solidification in mushy layers. 2011 *Phys. Fluids*, **23**, 016602.
16. Hitchen JR. 2018 *Understanding the growth and convective instability of mushy layers, with application to young sea ice*. PhD thesis, University of Oxford.
17. Worster MG. 1986 Solidification of an alloy from a cooled boundary. *J. Fluid Mech.*, **167**, 481–501.
18. Gewecke NR, Schulze TP. 2011 The rapid advance and slow retreat of a mushy zone. *J. Fluid Mech.*, **674**, 1–17.
19. Perovich DK, Richter-Menge JA. 1994 Surface characteristics of lead ice. *J. Geophys. Res.*, **99**, 16341–16350.
20. Huppert HE, Worster MG. 2012 Flows involving phase change. In *Handbook of Environmental Fluid Dynamics*, (ed. HJ Fernando). Boca Raton, FL: CRC Press.
21. Schulze TP, Worster MG. 2005 A time-dependent formulation of the mushy-zone free-boundary problem. *J. Fluid Mech.*, **541**, 193–202.
22. Peppin SSL, Huppert HE, Worster MG. 2008 Steady-state solidification of aqueous ammonium chloride. *J. Fluid Mech.*, **599**, 465–476.
23. Whiteoak SH, Huppert HE, Worster MG. 2008 Conditions for defect-free solidification of aqueous ammonium chloride in a quasi two-dimensional directional solidification facility. *J. Cryst. Growth*, **310**, 3545–3551.
24. Solomon TH, Hartley RR. 1998 Measurements of the temperature field of mushy and liquid regions during solidification of aqueous ammonium chloride. *J. Fluid Mech.*, **358**, 87–106.
25. O'Rourke JG, Riggs AJE, Guertler CA, Miller PW, Padhi CM, Popelka MM, Wells AJ, West AC, Zhong J-Q, Wettlaufer JS. 2012 Mushy-layer dynamics in micro and hyper gravity. *Phys. Fluids*, **24**, 103305.
26. Middleton CA, Thomas C, De Wit A, Tison J-L. 2016 Visualizing brine channel development and convective processes during artificial sea-ice growth using Schlieren optical methods. *J. Glaciol.*, **62**(231), 1–17.
27. Eide LI, Martin S. 1975 The formation of brine drainage features in young sea ice. *J. Glaciol.*, **14**, 137.
28. Galley RJ, Else BGT, Geilfus NX, Hare AA, Isleifson S, Barber DG, Rysgaard S. 2015 Imaged

brine inclusions in young sea ice-Shape, distribution and formation timing. *Cold Reg. Sci. Technol.*, **111**, 39–48.
29. Aussillous P, Sederman AJ, Gladden LF, Huppert HE, Worster MG. 2006 Magnetic resonance imaging of structure and convection in solidifying mushy layers. *J. Fluid Mech.*, **552**, 99–125.
30. Tait S, Jaupart C. 1992 Compositional convection in a reactive crystalline mush and melt differentiation. *J. Geophys. Res.*, **97**, 6735–6756.
31. Gough A, Mahoney A, Langhorne P, Williams M, Robinson N, Haskell T. 2012 Signatures of supercooling: McMurdo Sound platelet ice. *J. Glaciol.*, **58**, 38.
32. Roper SM, Davis SH, Voorhees PW. 2008 An analysis of convection in a mushy layer with a deformable permeable interface. *J. Fluid Mech.*, **596**, 333–352.
33. Neufeld JA, Wettlaufer JS. 2008 Shear-enhanced convection in a mushy layer. *J. Fluid Mech.*, **612**, 339–361.
34. Neufeld JA, Wettlaufer JS. 2008 An experimental study of shear-enhanced convection in a mushy layer. *J. Fluid Mech.*, **612**, 363–385.
35. Feltham DL, Worster MG. 1999 Flow-induced morphological instability of a mushy layer. *J. Fluid Mech.*, **391**, 337–357.
36. Neufeld JA, Wettlaufer JS, Feltham DL, Worster MG. 2006 Corrigendum. *J. Fluid Mech.*, **549**, 442.
37. Guba P, Worster MG. 2006 Nonlinear oscillatory convection in mushy layers. *J. Fluid Mech.*, **553**, 419–443.
38. Guba P, Worster MG. 2010 Interactions between steady and oscillatory convection in mushy layers. *J. Fluid Mech.*, **645**, 411–434.
39. Schulze TP, Worster MG. 1998 A numerical investigation of steady convection in mushy layers during the directional solidification of binary alloys. *J. Fluid Mech.*, **356**, 199–220.
40. Chung CA, Worster MG. 2002 Steady-state chimneys in a mushy layer. *J. Fluid Mech.*, **455**, 387.
41. Wells AJ, Wettlaufer JS, Orszag SA. 2010 Maximal potential energy transport: A variational principle for solidification problems. *Phys. Rev. Lett.*, **105**(25), 1–4.
42. Kerswell RR. 2018 Nonlinear nonmodal stability theory. *Annu. Rev. Fluid Mech.*, **50**, 319–345.
43. Doering CR, Gibbon JD. 1995 *Applied Analysis of the Navier-Stokes Equations*. Cambridge University Press.
44. Guba P, Anderson DM. 2017 Pattern selection in ternary mushy layers. *J. Fluid Mech.*, **825**, 853–886.
45. Hitchen JR, Wells AJ. 2016 The impact of imperfect heat transfer on the convective instability of a thermal boundary layer in a porous media. *J. Fluid Mech.*, **794**, 154–174.
46. Emms PW, Fowler AC. 1994 Compositional convection in the solidification of binary alloys. *J. Fluid Mech.*, **262**, 111–139.
47. Hwang IG, Choi CK. 2008 Onset of convection in a porous mush during binary solidification. *Korean J. Chem. Eng.*, **25**, 199–202.
48. Hwang IG. 2013 Stability analysis of compositional convection in a mushy layer in the time-dependent solidification system. *Korean J. Chem. Eng.*, **30**, 1023–1028.
49. Wettlaufer JS, Worster MG, Huppert HE. 1997 Natural convection during solidification of an alloy from above with application to the evolution of sea ice. *J. Fluid Mech.*, **344**, 291–316.
50. Wettlaufer JS, Worster MG, Huppert HE. 2000 Solidification of leads: Theory, experiment, and field observations. *J. Geophys. Res.*, **105**, 1123–1134.
51. Wells AJ, Wettlaufer, JS, Orszag SA. 2013 Nonlinear mushy-layer convection with chimneys: stability and optimal solute fluxes. *J. Fluid Mech.*, **716**, 203–227.
52. Wells AJ, Wettlaufer JS, Orszag SA. 2011 Brine fluxes from growing sea ice. *Geophys. Res. Lett.*, **38**, L04501.
53. Rees Jones DW, Worster MG. 2013 Fluxes through steady chimneys in a mushy layer during binary alloy solidification. *J. Fluid Mech.*, **714**, 127.
54. Rees Jones DW, Worster MG. 2013 A simple dynamical model for gravity drainage of brine from growing sea ice. *Geophys. Res. Lett.*, **40**, 307.
55. Katz RF, Worster MG. 2008 Simulation of directional solidification, thermochemical convection, and chimney formation in a Hele-Shaw cell. *J. Comput. Phys.*, **227**, 9823–9840.
56. Martin DF, Colella P, Graves D. 2008 A cell-centered adaptive projection method for the incompressible Navier-Stokes equations in three dimensions. *J. Comput. Phys.*, **227**, 1863–1886.
57. Heinrich JC, Poirier DR. 2004 Convection modeling in directional solidification. *C. R. Mécanique*, **332**, 429–445.

58. McPhee MG. 2008 *Air-Ice-Ocean Interaction: Turbulent Ocean Boundary Layer Exchange Processes*. Springer.
59. Shcherbina AY, Talley LD, Rudnick DL. 2003 Direct observations of North Pacific ventilation: brine rejection in the Okhotsk Sea. *Science*, **302**, 1952–1955.
60. Abernathey RP, Cerovecki I, Holland PR, Newsom E, Mazloff M, Talley LD. 2016 Water-mass transformation by sea ice in the upper branch of the Southern Ocean overturning. *Nature Geosci*, **9**, 596–601.
61. Widell K, Fer I, Haugan PM. 2006 Salt release from warming sea ice. *Geophys. Res. Lett.*, **33**, GL026262.
62. Jardon FP, Vivier F, Vancoppenolle M, Lourenço A, Bouruet-Aubertot P, Cuypers Y. 2013 Full-depth desalination of warm sea ice. *J. Geophys. Res. Oceans*, **118**, 435–447.
63. Peterson AK. 2018 Observations of brine plumes below melting Arctic sea ice. *Ocean Sci.*, **14**, 127–138.
64. Moreau S, Vancoppenolle M, Zhou J, Tison J-L, Delille B, Goosse H. 2014 Modelling argon dynamics in first-year sea ice. *Ocean Modelling*, **73**, 1–18.